BIBECHANA
Vol. 23, No. 3, August 2026, 75–82

ISSN 2091-0762 (Print), 2382-5340 (Online)
Journal homepage: http://nepjol.info/index.php/BIBECHANA
Publisher:Dept. of Phys., Mahendra Morang A. M. Campus (Tribhuvan University)Biratnagar

Evaluating aftershock decay behavior in the Central Himalaya via the modified Omori law

Rudra Prasad Poudel[1,2], Ram Krishna Tiwari[1*], Udaya Bahadur Thapa Kshetri[1,2] Eak Raj Paudel[1,2], Hari Har Paudyal[1]

[1]*Birendra Multiple Campus, Tribhuvan University, Kirtipur, Nepal.*
[2]*Central Department of Physics, Tribhuvan University, Kirtipur, Nepal.*

[*]Corresponding author: Email: ram.tiwari@bimc.tu.edu.np

Abstract

Omori's law is a fundamental concept that explains the temporal decay of aftershock activity. In this study, we applied a reformulated modified Omori law expressed as a differential equation to quantify the decay rate of aftershock behavior in the Central Himalaya. The key parameter, the deactivation coefficient (σ), quantifies how fast the earthquake sequence decays. Moreover, σ provides insight into post-seismic processes such as stress redistribution and microfracture healing. Aftershock sequences from three 2015 Central Himalayan earthquakes (Gorkha M7.6, Dolakha M7.0, and Kalikot M5.5) were analyzed using data from the International Seismological Center (ISC) and published catalogs. Since σ is a time-dependent function following the Omori epoch, only the initial 5–10 days after the mainshock were considered in this study. The results show that larger earthquakes exhibit smaller σ values: 0.012 ± 0.002 *for M7.6,* 0.022 ± 0.010 *for M7.0, and* 0.039 ± 0.012 *for M5.5, indicating slower and longer-lasting aftershock activity. The relation between mainshock magnitude and σ is consistent with the model $\sigma = A - BM_0$, although higher values of A (0.11) and B (0.01) were obtained. Compared to global observations, the Central Himalaya region exhibits slower post-seismic relaxation. This behavior is likely controlled by the low-angle geometry of the Main Himalayan Thrust, elevated pore fluid pressure, and complex fault structures. The apparent directional migration of aftershocks (eastward in eastern events and westward in western events) may indicate a partially locked or segmented section of the Main Himalayan Thrust, suggesting possible stress accumulation and a seismic gap in the Central Himalaya. These findings provide important implications for seismic hazard assessment, disaster preparedness, and risk mitigation strategies in the Central Himalaya region.*

Keywords
Deactivation constant; aftershocks; Modified Omori law; Omori-Utsu law; Himalayan seismicity.

Article information
Manuscript received: June 09, 2026; Revised: July 28, 2026; Accepted: July 31, 2026
DOI: https://doi.org/10.3126/bibechana.v23i3.95572
This work is licensed under the Creative Commons CC BY-NC License. https://creativecommons.org/licenses/by-nc/4.0/

1 Introduction

Aftershocks are common after mainshocks, representing the adjustment of the Earth's crust after mainshocks. The temporal decay of aftershocks related to interpreting the stress redistribution process in the lithosphere is important for understanding seismic hazard assessment [1, 2]. Although Omori's law describes the decay nature of aftershocks, it does not describe the physical mechanism related to the internal process in the lithosphere [3]. Recent developments have focused on reformulating the empirical law to make a better understanding of aftershocks related to source processes. The Himalaya is one of the active seismic regions due to the thrust between the Indian and Eurasian plates. Here, the Central Himalaya is selected as the area to study aftershocks to find the common trends of the region [4–6].

1.1 Classical aftershock theory and physical reformulation

Omori's law (1894) provides a fundamental framework for understanding aftershock activity and the temporal decay of seismic sequences. It describes the decay of the aftershock rate $n(t)$ with time t [7] as

$$n(t) = \frac{k}{c+t} \tag{1}$$

where k is the productivity constant controlling the initial aftershock rate, and c is the time offset parameter that accounts for the incompleteness of the catalog immediately after the main shock. Zavyalov (2022) reformulated this empirical relation into a physical differential equation that describes the temporal decay of aftershock activity associated with a main shock. This reformulation transforms Omori's law from a purely empirical expression into a representation of an underlying physical process governing aftershock decay.

$$\frac{dn}{dt} + \sigma n^2 = 0 \tag{2}$$

where σ is the deactivation coefficient, which quantifies the rate at which the earthquake source relaxes after the mainshock. A smaller value of σ indicates longer-lasting and more persistent aftershock activity.

The parameter σ may vary due to external influences such as stress transfer, geomagnetic effects, or tidal forcing. In the diffusion model, the aftershock zone migrates slowly with time, implying that the deactivation coefficient may be time-dependent, i.e., $\sigma = \sigma(t)$. To simplify the analysis, a new time variable τ is introduced as

$$\tau(t) = \int_0^t \sigma(t')\,dt' \tag{3}$$

Using this transformation, equation (2) becomes

$$\frac{dn}{d\tau} + n^2 = 0 \tag{4}$$

Integrating over the interval τ gives

$$\int_{n(0)}^{n(\tau)} \frac{dn}{n^2} = -\int_0^{\tau} d\tau \tag{5}$$

This formulation links Omori's empirical law to a dynamic physical process rather than a simple empirical fitting relation. Rearranging the equation, it can be expressed as

$$n(\tau) = \frac{n(0)}{1 + n(0)\displaystyle\int_0^t \sigma(t')\,dt'} \tag{6}$$

This formulation can be used to model a nonstationary deactivation rate after a large earthquake that may change due to transient triggers, variations in pore pressure, dynamic stressing, and related processes. All these effects are captured in $\sigma(t)$ and thus in $\tau(t)$. During the early phase after the mainshock, σ is approximately constant, referred to as the Omori epoch, during which Omori's classical hyperbolic decay is valid [9]. For constant σ, the equation reduces to the classical hyperbolic form given in Equation (2).

$$n(t) = \frac{n(0)}{1 + n_0 \sigma t} \tag{7}$$

Or equivalently,

$$\frac{1}{n(t)} = \frac{1}{n(0)} + \sigma t \tag{8}$$

This expression now has a direct physical interpretation. The equation is linear in $1/n(t)$ versus t, where the slope of the line provides σ, which can be estimated directly from aftershock data. It represents the initial constant deactivation rate within the Omori epoch.

1.2 Empirical σ–magnitude relationship

The regression between σ and earthquake magnitudes gives the dependence on the main shock magnitude M_0 [10]. This model links σ to the source relaxation rate as

$$\sigma = A - BM_0 \tag{9}$$

which in turn correlates with b-value and activity level. Both relations (modified Omori law and Gutenberg–Richter) are linear in M. Therefore, these values can be used for tectonic interpretation of a region. Here, we can interpret A and B as analogs of a and b, but describing temporal decay σ instead of spatial/magnitude frequency. The proportionality $(A - BM_0)$ quantifies that dependence globally. So, the pair (A, B) quantifies how energy release and relaxation scale with earthquake size [11].

The pair (A, B) serves as a regional mechanical fingerprint, characterizing how different crustal environments relax after large earthquakes. In the pair (A,B), A is the baseline deactivation, representing the overall relaxation level of the crust for a hypothetical zero-magnitude event. A higher value of A indicates faster aftershock decay regardless of magnitude. B represents the magnitude sensitivity, quantifying how strongly the deactivation coefficient decreases with increasing mainshock magnitude. A larger value of B implies strong magnitude dependence, meaning larger earthquakes decay much more slowly than smaller ones. A smaller B indicates weak magnitude dependence, so even moderate earthquakes decay quickly, and the decay rate does not vary strongly with magnitude. These values help to estimate when aftershocks drop below the background level and explain the post-seismic relaxation. Unlike the Gutenberg–Richter b-value, which characterizes the relative frequency of small versus large events, B characterizes how aftershock duration scales with mainshock size.

1.3 Tectonics of the study region

There is an ongoing collision between the Indian and Eurasian plates. This causes the region to fracture into many fault systems with the primary north-dipping Main Himalayan Thrust (MHT). The Central Himalaya, along with the thrust belt, is experiencing most seismic events [12–14]. The region is uplifted starting from the Ganga basin and is divided into structural zones called the Sub-Himalaya, Lesser Himalaya, Greater Himalaya, and the Tethys-Himalaya up to the South Tibetan Detachment (STD) [1,3]. Three recent earthquakes in the Himalayan region are analysed in this study.

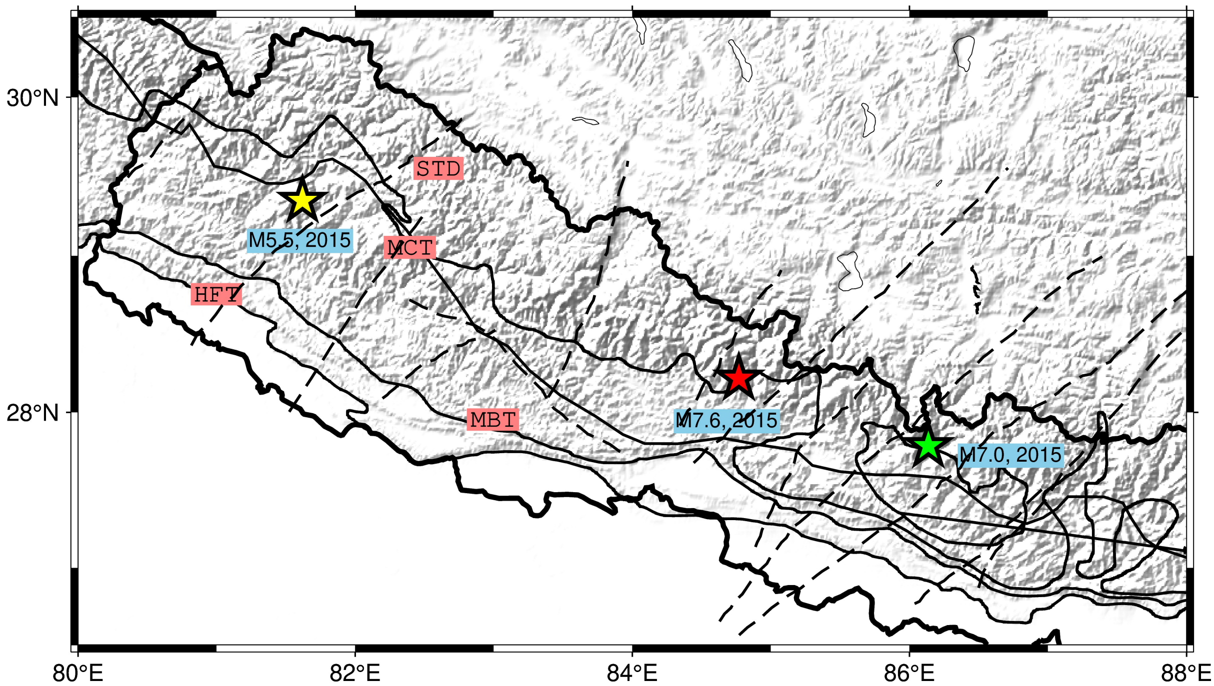

Figure 1: Central Himalaya regions showing three major past events (2015). Black continuous curves are the major faults, and dotted lines represent the cross faults in the region.

The major event occurred in the Gorkha district on 25 April 2015. The location has a latitude of 28.22° and longitude of 84.77° with a magnitude of 7.6 [1]. After that, another big event hit the Dolakha district on 12 May 2015 with a magnitude of 7.3. The epicenter was towards the east from the Gorkha epicenter, with latitude 27.79° and longitude 86.14°. The next event in the same year was a moderate event of magnitude 5.5 in Kalikot, western part of Nepal, with latitude 29.35° and longitude 81.62°. All three events occurred near the MCT in the same year 2015 [15]. Aftershocks of Gorkha migrated towards the east, while aftershocks of Dolakha (whose epicenter was east of the Gorkha epicenter) were scattered in all directions around its epicenter. On the other hand, the aftershocks due to the Kalikot earthquakes are very close to the epicenter, and some have migrated towards the west. The directional aftershock migration suggests a partially locked or segmented section of the MHT.

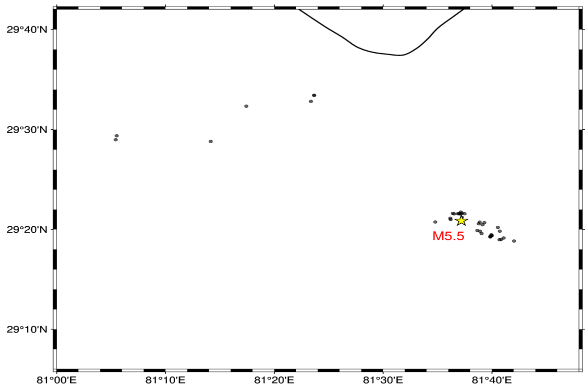

(a) Kalikot, $M = 5.5$

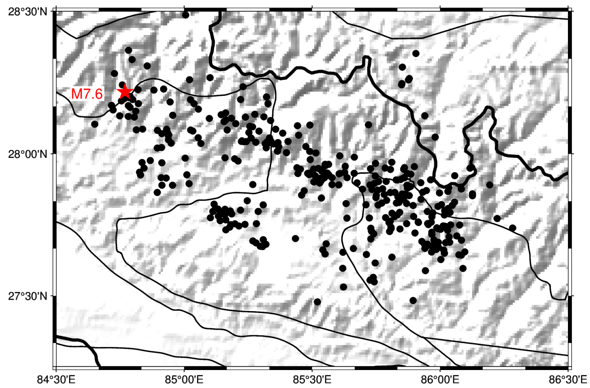

(b) Gorkha, $M = 7.6$

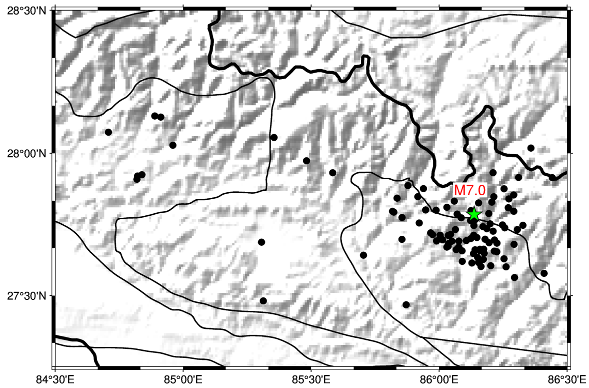

(c) Dolakha, $M = 7.0$

Figure 2: Main shocks and aftershocks in the Kalikot region [subplot (a)], Gorkha region [subplot (b)], and Dolakha region [subplot (c)]. Only aftershocks occurring within the respective calculation periods are included.

Due to varying size of main shocks and data limitaions, the data period for the Gorkha event was considered as 10 days, and for the other two events as 5 days, so that σ lies inside the Omori epoch. Since the active period of an aftershock sequence depends on the magnitude of the event, different time periods were used. Considering data limitations, only 5 days were considered for the other two events to balance the need for data quality. Figure 2 shows the aftershocks during the data observation period from the catalog. Since aftershocks are concentrated very close to the main shock location, the landscape is removed, and the map is zoomed for clarity, especially for the Kalikot event.

2 Data and methods

Data were downloaded from the International Seismological Center (ISC) catalog and a supplementary dataset [15,16]. The ZMAP Software in MATLAB was used to decluster the event data. For this, the time window of 1 day, a spatial tolerance of 10 km, and a 0.1 magnitude threshold were applied with the Reasenberg declustering algorithm. Then the events related to the three mainshocks were grouped for further analysis. Because aftershock activity decays rapidly for smaller events, a 5-day window was used for Kalikot M5.5 and Dolakha M7.0, while a 10-day window was used for the larger Gorkha M7.6 event. Within these windows, 52 were recorded for Kalikot, 102 for Dolakha, and 329 for Gorkha.

The data were binned into 1-day intervals. Weighted time was used for each bin along the time axis to account for the gradual decay of activity within each bin. The aftershock decay trends were analyzed using the modified Omori law to determine the source deactivation coefficient σ, which describes the temporal decay of aftershock activity. The relationship between mainshock magnitude and the deactivation coefficient was then plotted to estimate Zavyalov's parameters A and B (Equation 9), which were also compared with previously reported values [10].

3 Results and discussion

The spatial distribution of aftershocks relative to each mainshock is different for each event. For Gorkha (M 7.6), aftershocks are widely distributed along the Main Himalayan Thrust (MHT), and the aftershock activity is east of the mainshocks, showing stress transfer towards the east [17]. For Dolakha (M 7.0), aftershocks are scattered around the mainshock. Kalikot (M5.5) has tightly clustered aftershocks around the epicenter, consisting of a smaller rupture area, with some aftershocks toward the west. It supports the structural discontinuity in MHT as there is major structural discontinuity in the MHT around 82.5°E longitude [18,19]. Additional earthquake sequence analyses are required to confirm this possible interpretation. This limitation has now been explicitly stated in the Limitations section.

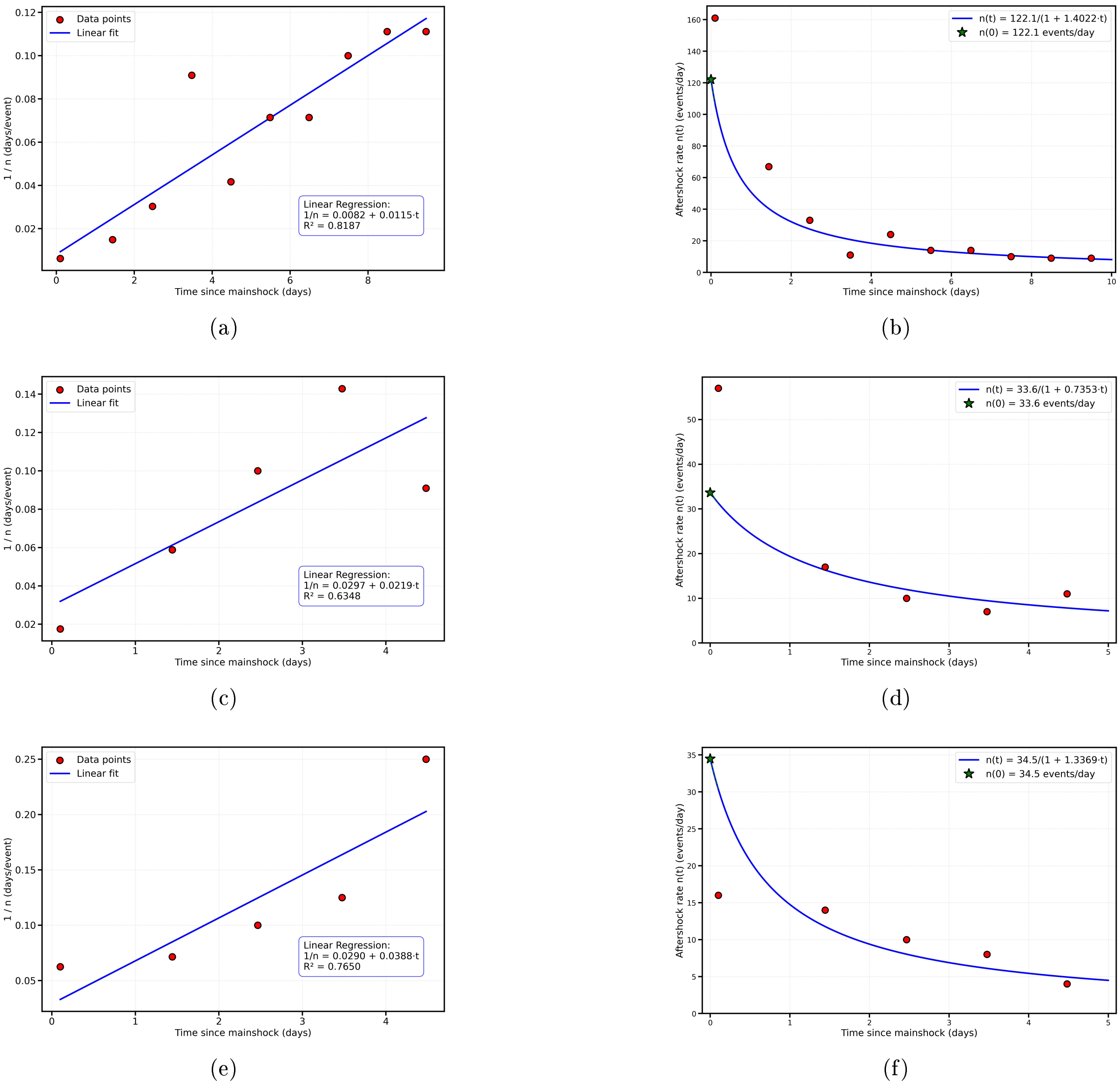

Figure 3: Aftershock analysis plots for different earthquake clusters (Kalikot, Gorkha, and Dolakha respectively). Subplots (a), (c), and (e) show the reciprocal of earthquake frequency versus time where as subplots (b), (d), and (f) present aftershock frequency versus time (days). The stars are the initial estimated activity of each main shocks. Weighted time for each bin of each day is used to plot along X-axis.

Table 1: Estimated Modified Omori law parameters for the analyzed earthquake sequences

Earthquake	M	n_0 (events/day)	σ (per event)	R^2
Gorkha	7.6	122.1 ± 28.5	0.012 ± 0.002	0.82
Dolakha	7.0	33.6 ± 10.8	0.022 ± 0.010	0.63
Kalikot	5.6	34.5 ± 14.8	0.039 ± 0.012	0.76

For each of the three mainshocks, the number of aftershocks versus time (days) is plotted. All the fits best explain the hyperbolic law. Then the reciprocal of aftershock frequency was plotted against time. These curves show a linear relationship with R^2 values of fit from 0.63 to 0.81. Results are summarized in Table 1. The initial aftershock rate $n(0)$ is higher for the largest mainshocks and smaller for other events. As expected from the Modified Omori law, the initial aftershock rate (n_0) increases with mainshock magnitude. The Gorkha earthquake (M 7.6) produced the highest initial aftershock rate (122.1 ± 28.5 events/day), whereas the Dolakha and Kalikot earthquakes produced substantially lower initial rates. This trend reflects the larger amount of stress released and the greater rupture area associated with larger earthquakes.

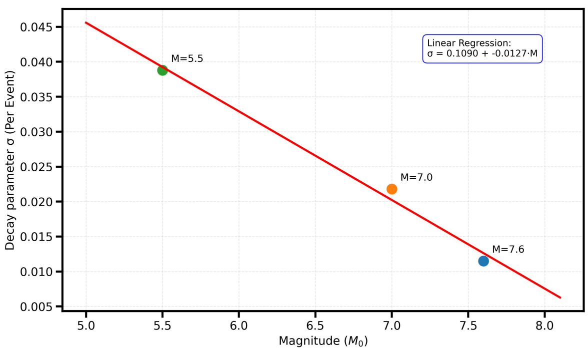

Figure 4: Deactivation coefficient σ as a function of mainshock magnitude M_0 for the three 2015 Central Himalayan events.

The deactivation coefficients (σ) are different for different earthquakes (Figure 3). The higher value of σ represents slower decay and vice versa. There is a clear decreasing trend with an increase in mainshock magnitude: 0.012 ± 0.002 for M7.6, 0.022 ± 0.010 for M7.0, and 0.039 ± 0.012 for M5.5, with R^2 values of 0.82, 0.63, and 0.76, respectively. For M7.0, the deactivation coefficient σ slightly increases, showing intermediate deactivation. The M5.5 event, which is moderate in comparison with the other two events (M7.6 and M7.0), has a higher deactivation rate, representing the fastest deactivation and shortest aftershock duration. The results completely satisfy the theoretical concept for seismic events as explained by the Omori law. Hence, a large earthquake takes a longer time for stress redistribution and fault relaxation.

Table 2: Comparison of regression parameters obtained in the present study and by Zavyalov et al. (2022).

Zavyalov et al. (2022)			Present work		
A	B	R^2	A	B	R^2
0.64	0.07	0.82	0.11	0.01	0.99

Decay parameter decreases linearly with main shock magnitude as shown in Figure ??. This explains that σ depends on the mainshock magnitude for $t > 0$. Our analysis confirms the linear σ–M_0 dependence reported by Zavyalov [8], supporting the source deactivation interpretation of the Omori law, while indicating region-specific differences in deactivation efficiency and magnitude sensitivity. For comparison these values are listed in Table 2. The smaller value of A can be due to regional tectonic conditions or fault properties. B value quantifies the measure of deactivation dependence on the size of the mainshock. A higher value of B is obtained than expected in this research. It represents higher deactivation of the aftershocks and higher stress migration of the earthquake. It explained that soon after the mainshock, the tectonic properties of the region became time functions and redistribution of stress occurred.

4 Conclusion

The seismically active Central Himalaya is always facing persistent seismic hazards. The main event in the region is followed by many aftershocks. Their frequency patterns provide valuable information about stress flow direction and mitigation strategies for future earthquakes. This study confirms the inverse relationship between the deactivation coefficient (σ) and mainshock magnitude (M_0) in the Central Himalaya, consistent with the physical reformulation of Omori's law [8]. Our results show that larger earthquakes (e.g., Gorkha M7.6) exhibit significantly smaller σ values (0.012), indicating more persistent aftershock sources and slower post-seismic relaxation, whereas smaller events (e.g., Kalikot M5.5) show larger σ (0.039), reflecting rapid deactivation. The observed aftershock pattern has regional differences that may suggest different seismic stress flow natures. The lower baseline deactivation (smaller A) and weaker magnitude sensitivity (smaller B) compared to global datasets suggest that the Himalayan active thrust environment, in comparison to global averaging, characterized by low-angle fault geometry, high pore fluid pressure, and complex fault branching [20–22] promotes longer aftershock durations. Spatially, larger mainshocks generate widely distributed aftershocks along the Main Himalayan Thrust (MHT), while smaller events produce tightly clustered sequences, consistent with rupture area scaling.

Overall, the observed linear decrease of σ with M_0 supports the interpretation of Omori's law as a source deactivation process. However, quantitative differences in fitted parameters highlight the importance of regional tectonics and dataset-specific effects. The σ–M_0 relationship offers practical value for seismic hazard assessment. For example, for a future event with magnitude 8.0, $\sigma = 0.008$ would complicate post-seismic recovery in the Central Himalaya. Despite limitations in catalog incompleteness and short time windows (5–10 days), our findings may require extended aftershock hazard assessments with more events to refine σ as a diagnostic tool for post-seismic relaxation. Our estimated σ values are generally smaller than those reported for intraplate or extensional settings [8], suggesting that the Himalayan thrust environment promotes longer aftershock durations.

Limitation of the study

This study is based on three major aftershock sequences from the 2015 Central Himalaya earthquakes. Although these events provide valuable insights into the temporal evolution of aftershock activity and the deactivation coefficient, the limited sample size reduces the statistical power of the regression analysis and restricts the generality of the proposed magnitude–σ relationship. Consequently, interpretations regarding directional aftershock migration should be regarded as preliminary. Future studies incorporating additional earthquake sequences from the Himalaya and other tectonic regions are needed to validate and refine these findings.

Acknowledgments

The author RPP would like to acknowledge the Tribhuvan University for providing sabbatical leave and we would also like to acknowledge Birendra Multiple Campus, Bharatpur, and the Central Department of Physics, Tribhuvan University, Kirtipur, Nepal, for their support.

Funding statement

This research received no external funding.

Conflicts of interest

The authors declare that there are no conflicts of interest associated with the publication of this research paper.

Author's contribution

RPP: Writing original draft. RKT: Conceptualisation. UBTC and ERP: Software support. HP: Reviewing and editing.

References

[1] Tiwari R, Paudyal H. Fractal structure of seismic signals of 2015 Gorkha-Kodari Earthquakes: A box counting method. BMC Journal of Scientific Research. 2022 12;5(1):18-26.

[2] Guo Y, Zhuang J, Ogata Y. Modeling and forecasting aftershocks can be improved by incorporating rupture geometry in the ETAS model. Geophysical Research Letters. 2019 10;46(22):12881-9.

[3] Thapa DR, Tao X, Fan F, Tao Z. Aftershock analysis of the 2015 Gorkha-Dolakha (Central Nepal) earthquake doublet. Heliyon. 2018 7;4(7):e00678.

[4] Morales-Yáñez C, Bustamante L, Benavente R, Sippl C, Moreno M. B-value variations in the Central Chile seismic gap assessed by a Bayesian transdimensional approach. Scientific Reports. 2022 12;12(1):21710.

[5] Tiwari RK, Paudyal H. Variability of b-value before and after the Gorkha earthquake in the Central Himalaya and Vicinity. Bibechana. 2021 2;18(2):32-42.

[6] Riesner M, Bollinger L, Hubbard J, Guérin C, Lefèvre M, Vallage A, et al. Localized extension in megathrust hanging wall following great earthquakes in western Nepal. Scientific Reports. 2021 11;11(1):21521.

[7] Utsu T, Ogata Y, S R, Matsu'ura. The centenary of the Omori formula for a decay law of aftershock activity. Journal of Physics of the Earth. 1995 1;43(1):1-33.

[8] Zavyalov A, Zotov O, Guglielmi A, Klain B. On the Omori Law in the Physics of Earthquakes. Applied Sciences. 2022;12(19):9965.

[9] Guglielmi A, Zavyalov A, Zotov O, Klain B. About the aftershocks, the Omori law, and the

Utsu formula. arXiv (Cornell University). 2023 5.

[10] Guglielmi A, Zotov O. Bifurcation of the earthquake source at the end of the Omori epoch. arXiv (Cornell University). 2023 3.

[11] Adhikari LB, Gautam UP, Koirala BP, Bhattarai M, Kandel T, Gupta RM, et al. The aftershock sequence of the 2015 April 25 Gorkha–Nepal earthquake. Geophysical Journal International. 2015 11;203(3):2119-24.

[12] Riesner M, Bollinger L, Hubbard J, Guérin C, Lefèvre M, Vallage A, et al. Localized extension in megathrust hanging wall following great earthquakes in western Nepal. Scientific Reports. 2021;11(1):21521.

[13] Kayal J. Microearthquake activity in some parts of the Himalaya and the tectonic model. Tectonophysics. 2001;339(3-4):331-51.

[14] Tiwari RK, Poudel RP, Paudyal H. Machine learning for predicting earthquake magnitudes in the Central Himalaya. Bibechana. 2025 1;22(1):22-9.

[15] Laporte M, Bollinger L, Lyon-Caen H, Hoste-Colomer R, Duverger C, Letort J, et al. Seismicity in far western Nepal reveals flats and ramps along the Main Himalayan Thrust. Geophysical Journal International. 2021 4;226(3):1747-63.

[16] International Seismological Centre. ISC-EHB Bulletin: Catalogue Search; 2026.

[17] Avouac JP, Meng L, Wei S, Wang T, Ampuero JP. Lower edge of locked Main Himalayan Thrust unzipped by the 2015 Gorkha earthquake. Nature Geoscience. 2015 8;8(9):708-11.

[18] Harvey JE, Burbank DW, Bookhagen B. Along-strike changes in Himalayan thrust geometry: Topographic and tectonic discontinuities in western Nepal. Lithosphere. 2015 6;7(5):511-8.

[19] Murphy MA, Taylor MH, Gosse J, Silver CRP, Whipp DM, Beaumont C. Limit of strain partitioning in the Himalaya marked by large earthquakes in western Nepal. Nature Geoscience. 2013 11;7(1):38-42.

[20] Zhou Z, Kusky TM, Tang CC. Coulomb stress change pattern and aftershock distributions associated with a blind low-angle megathrust fault, Nepalese Himalaya. Tectonophysics. 2019 7;767:228161.

[21] Scholz CH. The mechanics of earthquakes and faulting; 2002.

[22] Dyja-Person V, Tarantola A, Richard A, Hibsch C, Siebenaller L, Boiron MC, et al. Metamorphic brines and no surficial fluids trapped in the detachment footwall of a Metamorphic Core Complex (Nevado-Filábride units, Betics, Spain). Tectonophysics. 2018 2;727:56-72.